OAK RIDGE
NATIONAL LABORATORY
MANAGED BY UT-BATTELLE
FOR THE DEPARTMENT OF ENERGY

ORNL/TM-2012/254

High Temperature and Pressure Steam-H_2 Interaction with Candidate Advanced LWR Fuel Claddings

June 29, 2012

Prepared by
B. A. Pint
Corrosion Science & Technology Group Leader
Materials Science and Technology Division

UT-BATTELLE
ORNL-27 (4-00)

ORNL/TM-2012/254

Materials Science and Technology Division

HIGH TEMPERATURE AND PRESSURE STEAM-H_2 INTERACTION WITH CANDIDATE ADVANCED LWR FUEL CLADDINGS

B. A. Pint

Date Published: June 2012

Prepared by
OAK RIDGE NATIONAL LABORATORY
Oak Ridge, Tennessee 37831-6283
managed by
UT-BATTELLE, LLC
for the
U.S. DEPARTMENT OF ENERGY
under contract DE-AC05-00OR22725

CONTENTS

Page

LIST OF FIGURES

ACKNOWLEDGMENTS

The project team included J. R. Keiser, K. A. Terrani, M. P. Brady and T. Cheng. P. F. Tortorelli and K. L. More assisted with the SiC characterization and interpretation of results. The experimental work was conducted by M. Howell, M. Stephens, T. Lowe, H. Longmire, J. Mayotte and T. Jordan at ORNL. P. F. Tortorelli and L. L. Snead provided useful comments on the draft manuscript. This research was funded by the U.S. Department of Energy's Office of Nuclear Energy, Advanced Fuel Campaign of the Fuel Cycle R&D program and the Office of Basic Energy Sciences, Shared Research Equipment User Facility.

ABSTRACT

This report summarizes the work completed to evaluate cladding materials that could serve as improvements to Zircaloy in terms of accident tolerance. This testing involved oxidation resistance to steam or H_2-50%steam environments at 800°-1350°C at 1-20bar for short times. A selection of conventional alloys, SiC-based ceramics and model alloys were used to explore a wide range of materials options and provide guidance for future materials development work. Typically, the SiC-based ceramic materials, alumina-forming alloys and Fe-Cr alloys with ≥25%Cr showed the best potential for oxidation resistance at ≥1200°C. At 1350°C, FeCrAl alloys and SiC remained oxidation resistant in steam. Conventional austenitic steels do not have sufficient oxidation resistance with only ~18Cr-10Ni. Higher alloyed type 310 stainless steel is protective but Ni is not a desirable alloy addition for this application and high Cr contents raise concern about α' formation. Higher pressures (up to 20.7 bar) and H_2 additions appeared to have a limited effect on the oxidation behavior of the most oxidation resistant alloys but higher pressures accelerated the maximum metal loss for less oxidation resistant steels and less metal loss was observed in a H_2-50%H_2O environment at 10.3 bar. As some of the results regarding low-alloyed FeCrAl and Fe-Cr alloys were unexpected, further work is needed to fundamentally understand the minimum Cr and Al alloy contents needed for protective behavior in these environments in order to assist in alloy selection and guide alloy development.

1. INTRODUCTION

To provide larger safety margins and potentially avoid future nuclear disasters like the March 2011 accident in Japan, one strategy is to develop fuel systems that tolerate severe accident conditions better than the current Zircaloy/UO_2 fuel rods. Under severe accident scenarios in light water reactors (LWRs), e.g. loss of coolant accidents and station blackout, the fuel could become exposed; under these conditions the drop in heat conductance from the fuel coupled with decay heat production quickly drives the fuel temperature upward. In the case of conventional LWR fuel, the increase in temperature causes the zirconium alloy cladding to burst at temperatures between 800 to 1100ºC depending on the rod internal pressure. At temperatures above ~1200ºC, enthalpy production due to oxidation of zirconium significantly adds to the heat production rate in the core; a self-catalytic phenomenon that quickly surpasses the decay heat production rate in magnitude and results in rapid production of hydrogen as the byproduct of reaction of zirconium with steam.

An example alternative material is a ceramic clad fuel using SiC composites[1-3], which could survive much higher temperatures than Zircaloy. While a ceramic cladding has the potential to be protective above 1500°C, where ferrous alloys would melt, SiC is difficult to fabricate and has lower ductility than a metallic cladding. Also, the thin SiO_2 layer that forms on SiC is known to be less protective in the presence of water vapor because of the formation of hydroxides[4]. Thus, another strategy is to return to stainless steel claddings that were previously used as fuel cladding, despite the neutronics performance penalty during normal operation compared to Zircaloy[5]. Composition guidelines are needed in order to identify compositions capable of forming protective scales at temperatures of 1200°C and higher for relatively short (<24 h) periods to simulate accident conditions. The goal of this work was to compare the performance of Zircaloy, SiC and various Fe-base alloys in steam and steam-H_2 environments at 800°-1350°C and 1-20 bar. Conventional wrought, oxide dispersion strengthened (ODS) and model alloys were exposed to simulated conditions for 2-48 h in order to determine which classes of alloys are most attractive for further study. The most likely options are FeCrAl alloys with ~20wt.%Cr-5%Al and Fe-Cr alloys with ≥25%Cr alloys. However, further work could lower the Cr and Al contents. Conventional 304-type stainless steel claddings are more oxidation resistant than Zircaloy but do not contain sufficient Cr and Ni levels to be protective at 1200°C and higher temperatures.

2. EXPERIMENTAL PROCEDURE

Specimens evaluated in this study included sections of tubing with 0.65-1.6 mm wall thickness and coupons, typically 1-2mm thick and 4-6 cm^2 in surface area. Compositions are given in Table 1 in mass %. The baseline materials evaluated were tubing sections of Zircaloy-2 (0.9 mm thick wall), Zircaloy-4 (0.8mm), 304L (1.6mm), 321 (1mm), 347L (0.7mm) and 317L (1mm) and coupons of various SiC materials including Rohm & Haas chemical-vapor-deposited (CVD) SiC which is 99.99% pure SiC, NITE SiC[3], SiC/SiC composites with Nicalon fibers and reaction bonded SiC. Model binary and ternary alloys are referred to by their nominal composition but their actual compositions are given in Table 1. Oxidation exposures were conducted for 2-48h in 100% steam and H_2-50%H_2O at temperatures of 800°-1350°C and total pressures up to 20.7 bar (300 psi or 2MPa). A summary of the exposure conditions is given in Table 2 along with the flow rates which decreased from 95 cm/min at 3.4bar to 14cm/min at 20.7bar at 1200°C and increased at higher temperatures and decreased at lower temperatures. Multiple specimens were exposed in the high-pressure tests and were attached to a center alumina tube using Pt wire, Figure 1. For 800°-1000°C exposures, an alloy 230 (Ni-22Cr-14W) containment tube was used, while it was replaced with a SiC tube for 1200°-1350°C exposures. For thermal gravimetric analysis (TGA) using a Cahn model 1000 microbalance, a quartz tube was used with 1 bar of Ar-50%H_2O or dry air. In both the TGA and high-pressure rig, the gas flowed from the bottom to the top of the tube. Before and after exposure, specimen mass was measured using a Mettler-Toledo model XP205 balance with ±0.01mg/cm^2 accuracy. After exposure, specimens were metallographically sectioned and examined by light microscopy to determine section loss. Metal loss is reported as the average maximum values from three regions of the cross-sections. Characterization included x-ray diffraction, scanning electron microscopy (SEM) equipped with energy-dispersive x-ray analysis and transmission electron microscopy (TEM) with specimens prepared by focused ion beam milling.

Table 1. Alloy compositions (mass %) determined by inductively coupled plasma & combustion techniques

Alloy	Fe	Zr	Ni	Cr	Al	Mo	Mn	Si	C	O	S	Other
Zircaloy-2	0.14	98.1	0.05	0.10	-	-	-	0.01	0.019	0.115	<	1.42Sn
Zircaloy-4	0.22	98.2	-	0.11	-	-	-	0.01	0.016	0.118	<	1.27Sn
304L	70.3	-	8.27	18.8	0.01	0.27	0.73	0.42	0.028	0.006	<	
317L	64.2	-	11.86	18.9	-	3.13	0.62	0.38	0.023	0.006	10	
321	69.9	-	9.47	17.7	0.03	0.24	1.14	0.45	0.033	0.003	40	
347	68.9	-	9.97	17.5	-	0.16	1.80	0.66	0.040	0.007	150	
310SS	51.9	<	19.5	25.4		0.13	1.89	0.70	0.044	0.006	10	0.15Co,0.1Cu
AL6XN	48.2		24.1	20.4	0.01	5.98	0.50	0.05	0.012	0.003	<	0.2N,0.3Cu
Fe20Cr15Ni	65.3	<	15.3	19.4	<	<	<	0.01	0.002	0.043	47	
Fe20Cr20Ni	60.1	<	20.1	19.7	<	<	<	0.01	0.001	0.042	41	
Fe20Cr20Ni+	57.9	<	19.9	20.2	0.03	<	1.61	0.22	0.001	0.003	<	0.12La
Fe20Cr25Ni	55.4	<	24.8	19.5	<	<	<	<	0.002	0.043	45	
HR120	35.0	<	37.6	24.7	0.09	0.28	0.73	0.24	0.059	0.003	<	0.61Nb,0.2Cu
P91	88.7	<	0.16	8.75	0.03	0.98	0.46	0.28	0.102	0.004	30	0.46Nb,0.24V
Fe-15Cr	85.1	-	<	14.8	<	<	<	<	0.003	0.004	20	
Fe-20Cr	80.3	-	<	19.7	<	<	<	0.01	0.002	0.003	15	
Fe-25Cr	74.6	-	-	25.3	-	-	-	0.02	0.004	0.037	10	
ODM401	83.9	0.001	0.13	14.0	0.06	0.30	0.04	0.04	0.013	0.191	52	0.21Y,1.0Ti
E-Brite	72.6		0.13	25.8		1.00	<	0.22	0.003	0.003	100	0.1Nb,0.1V
AL294C	66.1		0.19	28.6	0.07	3.70	0.21	0.27	0.017	0.002	<	0.3Nb,0.37Ti
PM2000	74.6	-	0.1	18.9	5.1	0.01	0.11	0.04	0.01	0.25	8	0.37Y,0.45Ti
APMT	69.0	0.10	0.12	21.6	4.93	2.77	0.10	0.53	0.030	0.049	<	0.12Y,0.16Hf
Ohmaloy30	82.8	<	0.58	12.6	2.60	0.05	0.41	0.26	0.017	<	<3	0.34Ti,0.1V
Ohmaloy40	81.7	<	0.53	12.7	3.59	0.10	0.37	0.22	0.021	<	<3	0.34Ti,0.13V
NITE-SiC	0.32	-	0.04	0.09	0.38	-	-	67.8	27.7	2.94	<	0.44Y
CVD-SiC	-	-	0.01	-	-	-	-	69.8	30.2	0.003	<	-

Note: < denotes below the detectable limit of 0.01% or 0.001% for interstitials

Table 2. Overview of the high-pressure exposures completed

Temperature	Pressure (psig)	Gas	Flow (cm/min)	2h	5-6h	8h	18h	24h	48h
800°C	50	steam	67	X	X	X		X	
	100	H_2-H_2O				X			
	150	steam	15			X			
	150	H_2-H_2O	13			X			
1000°C	50	steam	79	X		X		X	
	100	H_2-H_2O	39			X			
	150	steam	22			X			
	150	H_2-H_2O	18			X			
1200°C	50	steam	95	X	X	X	X	X	X
	100	H_2-H_2O	46			X			
	150	steam	29	X		X		X	
	150	H_2-H_2O	21			X			
	300	steam	15	X		X		(fail)	
1300°C	50	steam	105			X			
	250	steam							X
1350°C	50	steam	111			X			

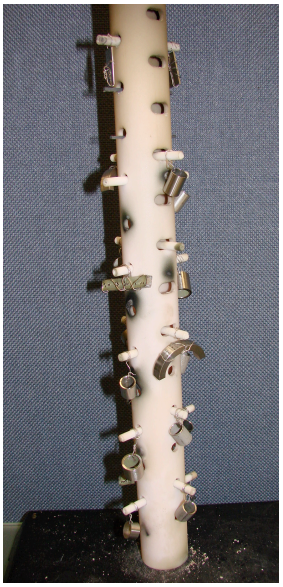

Fig. 1. Specimens were attached to alumina rods using Pt-Rh wire and the rods were slotted in a ~50mm diameter alumina tube that was loaded into the pressurized tube.

3. RESULTS

3.1 EFFECT OF TEMPERATURE

Figure 2 shows mass gain data after 8h exposures at 800°-1350°C for various alloys. The steam oxidation behavior of Zircaloy has been extensively studied[6-8] and will not be extensively reported here. Mass gains for Zircalloy-2 are shown in Figure 2 for reference to the more oxidation resistant alloys. The typical 18-8 stainless steels (i.e. 304L, 321L, 347) all performed similarly in these experiments and the mass change for 304L is shown for reference. The mass change for austenitic alloys is not as reliable because scale spallation is more likely for thick oxides because of their higher thermal expansion coefficient compared to ferritic alloys[9]. For example, 304L showed a mass loss at 1000°C because of scale spallation. (Recall that the mass gain for an adherent surface oxide is the uptake mass of oxygen while the mass loss for oxide spallation includes the oxygen and the heavier metal cations.) For these alloys, cross-sections are needed to assess the extent of attack, as will be shown later. Typical cross-sections of the less protective tubing alloys are shown in Figure 3. Most were fully consumed or nearly so after only 8h at 1200°C. In contrast, the most oxidation resistant materials examined over this temperature range were FeCrAl, such as Kanthal APMT (Table 1), which is a powder metallurgy alloy with some high temperature strength due to its oxide dispersion. This material showed a low mass gain even at 1350°C due to the formation of a protective alumina scale, which is less affected by H_2O than SiO_2 or Cr_2O_3[4]. As a representative of the various SiC composites, CVD SiC also showed low mass changes from 800°-1350°C, Figure 2. Another class of alloys of interest are the ferritic steels and two examples are shown, a model binary alloy Fe-25Cr and a commercial (Allegheny Ludlum) alloy AL294C (Fe-29Cr-4Mo). Both showed increased attack above 1200°C. The most oxidation resistant materials begin to strongly differentiate at 1200°C so more attention will be focused on the highest temperature results and less devoted to the range of experiments conducted at 800° and 1000°C where thinner reaction products were formed and less differentiation occurred among the various alloys.

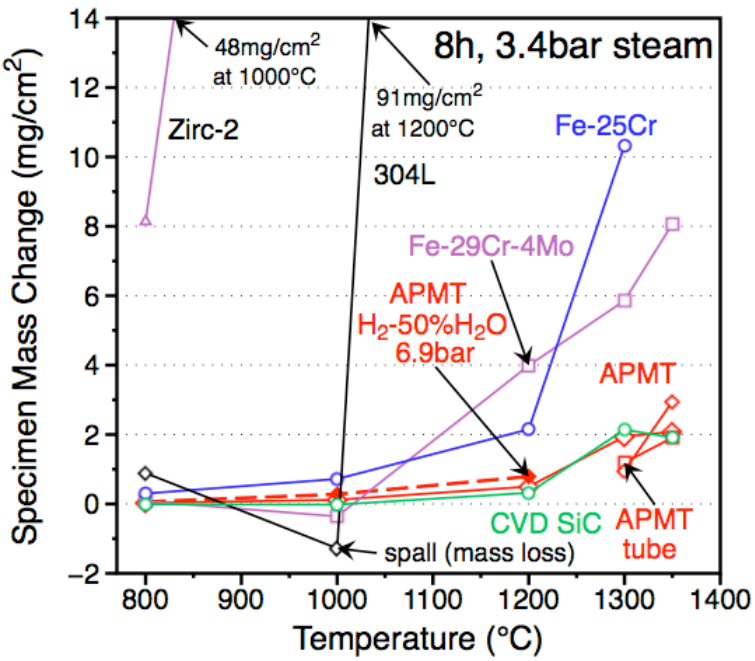

Fig. 2. Specimen mass change data after exposures in 3.4 bar steam as a function of temperature for 8h exposures. Additional data is included for 6.9 bar H_2-50%H_2O for alloy APMT (dashed line).

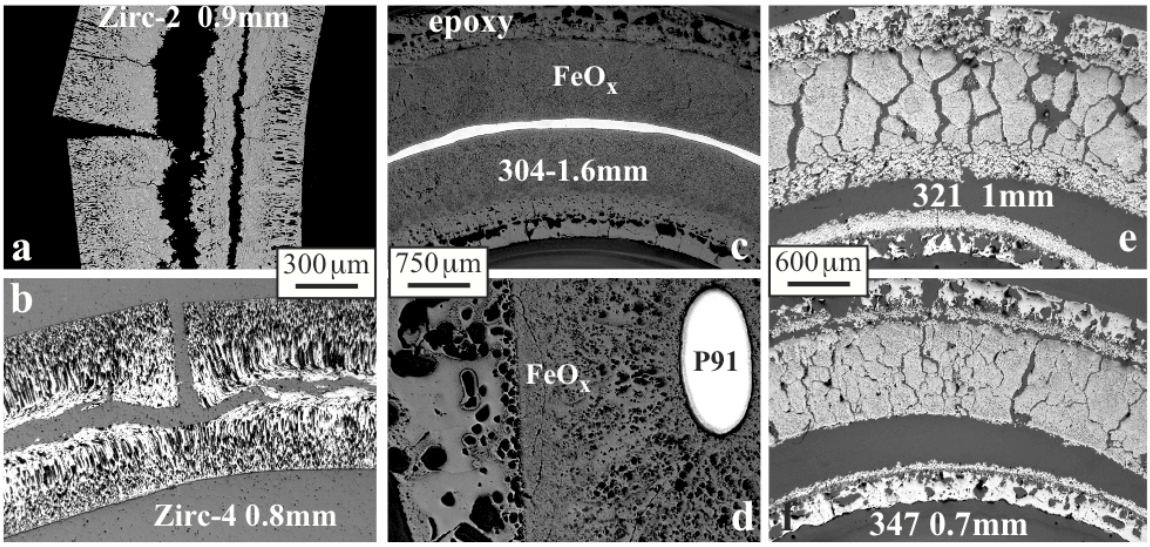

Fig. 3. Example cross-sections of the less oxidation resistant tubing alloys exposed for 8h at 1200°C in 10.3bar (150psi) including (a) Zircaloy 2, (b) Zircaloy 4, (c) type 304, (d) P91, (e) type 321 and (f) type 347 stainless steel.

Figure 4 shows example cross-sections of the oxides formed on APMT and CVD SiC at the highest temperatures investigated in this study. Figure 4a shows the protective external alumina scale formed on APMT after 48h at 1200°C in 3.4bar steam. Figures 4b and 4c show APMT after 8h at 1300° and 1350°C, respectively. In each case, the alumina forms a solid-state diffusion barrier that limits the oxidation rate to ionic diffusion (mainly anions) through this oxide layer, which is relatively inert to the presence of steam. The reactive element (RE) additions of Y and Hf in this alloy are essential to the good scale adhesion observed[10,11]. Since the RE additions are mainly tied up as oxides in this alloy, there is virtually no internal oxidation observed at these temperatures. For comparison, the SiO_2 layer formed on CVD SiC at 1350°C is shown in Figure 4d. With the relatively low gas velocities and the presence of $Si(OH)_4$ vapor due to reaction of the SiC containment tube, only limited volatilization occurred in this case and the layer is therefore thicker than it would be in a test with higher gas velocity[12].

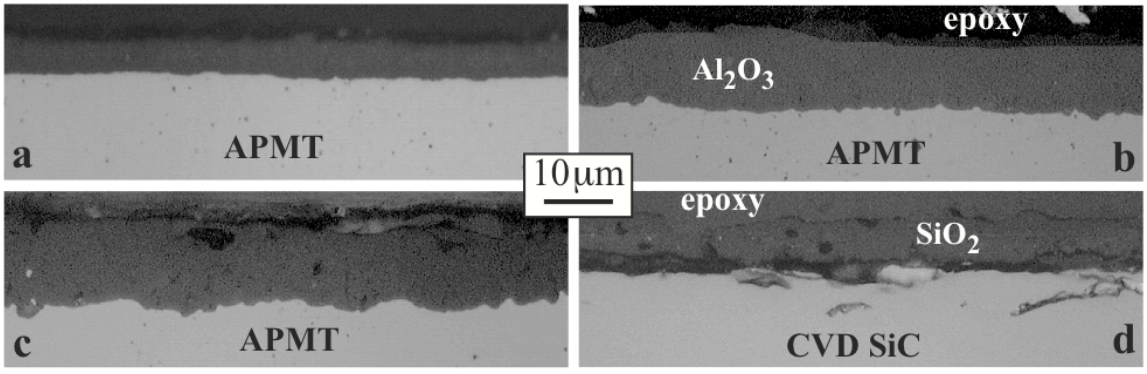

Fig. 4. Light microscopy of polished cross-sections of APMT after exposure in 3.4 bar steam for (a) 48h at 1200°C, (b) 8h at 1300°C and (c) 8h at 1350°C and (d) CVD SiC after 8h at 1350°C.

3.2 OXIDATION BEHAVIOR OF SiC-BASED SPECIMENS

The oxidation of SiC materials in combustion environments with small amounts of water vapor has been studied extensively.[12-16] Under these conditions, paralinear oxidation kinetics have been observed. Effectively, material recession is governed by the two-step process of silica scale formation on the surface of SiC and silica layer volatilization upon further reaction of this layer with steam to form volatile species (e.g. hydroxides). The former process is governed by parabolic kinetics of the diffusion of the oxidizing species through the oxide layer whereas the volatilization process exhibits linear kinetics. At long times, the oxide layer reaches a steady state thickness and the material recession rate is governed by the volatilization step[17]. The kinetics of volatilization is governed by the transport of the volatile species from the oxide surface to the bulk gas stream and is dependent on the flow conditions. Under laminar flow and assuming flat sample geometry the flux of volatile species through the gas boundary layer is as follows[12]:

$$J \propto \frac{v^{1/2}}{P_{total}^{1/2}} \sum P_{volatile} \qquad (1)$$

where v is the gas velocity in the bulk and P is the pressure. The volatile species pressure has a specific dependence on the steam pressure that can be determined from the particular chemical reaction that governs volatilization. If the following chemical reaction governs the surface volatilization reaction, then the law of mass action implies the volatile pressure at the gas-solid interface is proportional to the square of the steam pressure.

$$2H_2O_{(g)} + SiO_{2(s)} \rightarrow Si(OH)_{4(g)} \qquad (2)$$

Given that the total pressure in the system is dominated by the steam partial pressure (the partial pressure of other species is negligible), Eq. 1 implies that the transport of volatile species across the gas boundary layer is proportional to $v^{1/2}P^{3/2}$. Note that slight deviations from this ideal scenario are expected when one considers steam flow against the cylindrical geometry of fuel-cladding materials (e.g. SiC cladding) within the coolant channels inside the reactor core.

Figure 5 shows the results under various conditions for CVD SiC specimens as a surrogate for the more complex composite specimens. The extent of material recession is normalized against the $v^{1/2}P^{3/2}$ parameter. The gas flow rates varied as shown in Table 2. As expected, the increase in temperature results in faster recession kinetics, Figure 5a. Figure 5b indicates that the material recession is likely governed by linear volatilization kinetics as plotting the material loss values against the $v^{1/2}P^{3/2}$ shows good agreement with the mechanism discussed above.

In order to further understand these observations, additional characterization was performed on the SiO_2 reaction product that formed on CVD SiC. Figures 6 and 7 show SEM and TEM of the reaction products under various conditions. The outer layer was porous cristobalite while the inner layer was denser and amorphous at both 1200° and 1350°C, Figure 6. This structure is typical of what was observed in earlier studies of SiC/SiC composites that were developed for gas turbine combustor liners[15,16]. The amorphous structure of the inner layer was confirmed using TEM, Figure 7.

The NITE SiC[3] recession kinetics differed from what was observed for CVD SiC. Figure 8 shows the extent of material recession as a function of time at 1200°C at 3.4 bar steam pressure for CVD SiC, NITE SiC, and APMT. The NITE SiC kinetics did not follow linear kinetics (a parabolic fit was assigned in Figure 8). This is likely due to the Al and Y additions (Table 1) being incorporated into the surface reaction product and being enriched with time as the Si evaporates. Figure 9 shows SEM cross-sections of the surface reaction product formed on NITE. Especially at

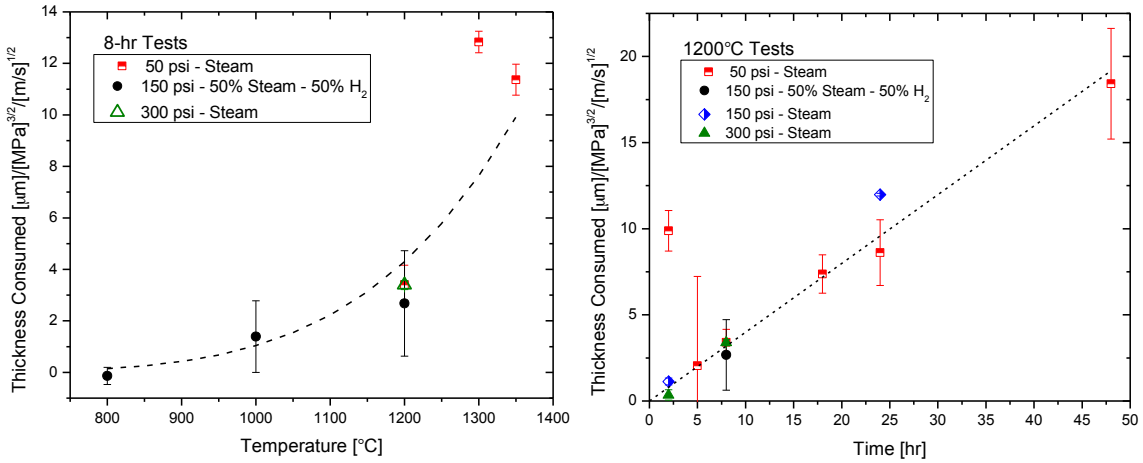

Fig. 5. CVD SiC recession at various steam pressures: (a) as a function of temperature during 8 h exposures and (b) as a function of time at 1200°C.

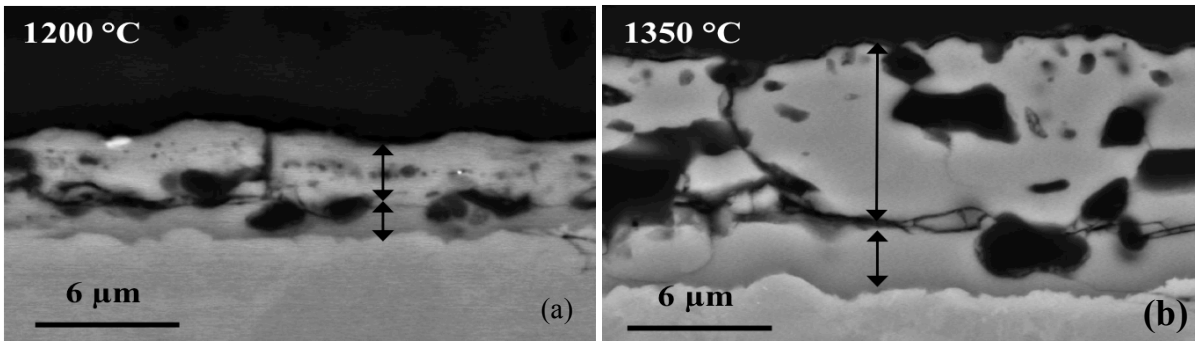

Fig. 6. SEM backscattered electron images of the scale formed on CVD SiC after 8h in 3.4 bar steam (a) 1200°C and (b) 1350°C.

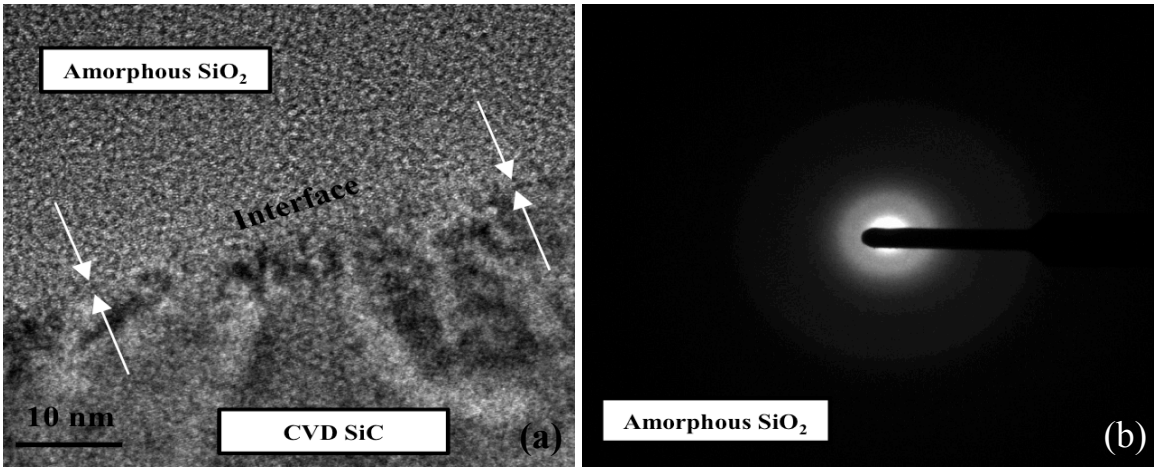

Fig. 7. (a) TEM annular dark field image of the CVD-SiC/SiO_2 interface formed after 8h at 1200°C in 3.4 bar steam. In (b), the TEM selected area diffraction pattern without spots indicates amorphous SiO_2.

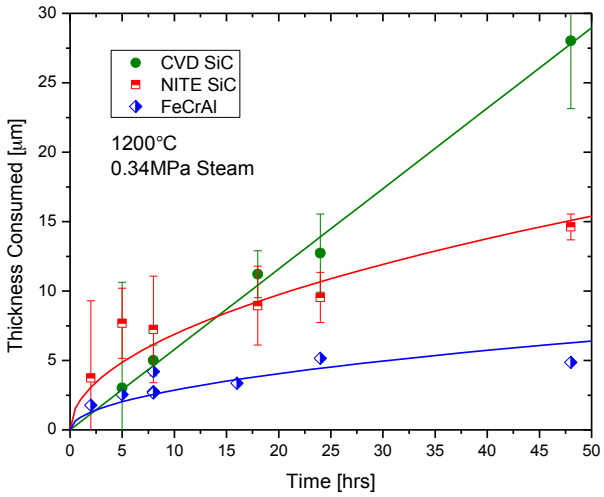

Fig. 8. Material recession as a function of time at 1200°C at 50psi steam. Kanthal alloy APMT is designated as FeCrAl.

1200°C, Figure 9c, the oxide appears substantially different than that observed on CVD SiC, e.g. Figures 4d and 6a. For a further comparison, Figure 10 shows X-ray diffraction results comparing the oxides formed on CVD and NITE SiC after 5h at 1200°C in 3.4bar steam. A larger cristobalite peak was observed for the NITE specimen suggesting that more of the reaction product was crystalline on the NITE SiC.

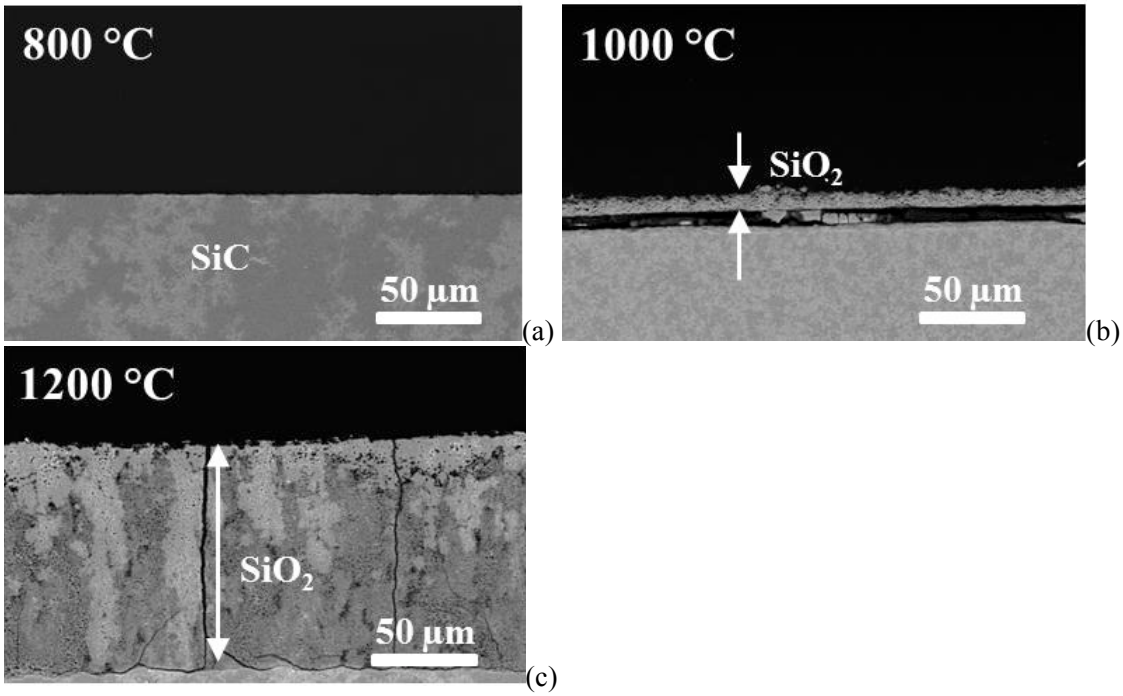

Fig. 9. SEM secondary electron images of NITE SiC cross sections after exposure in 10.3 bar steam for 8 h at (a) 800°C, (b) 1000°C and (c) 1200°C.

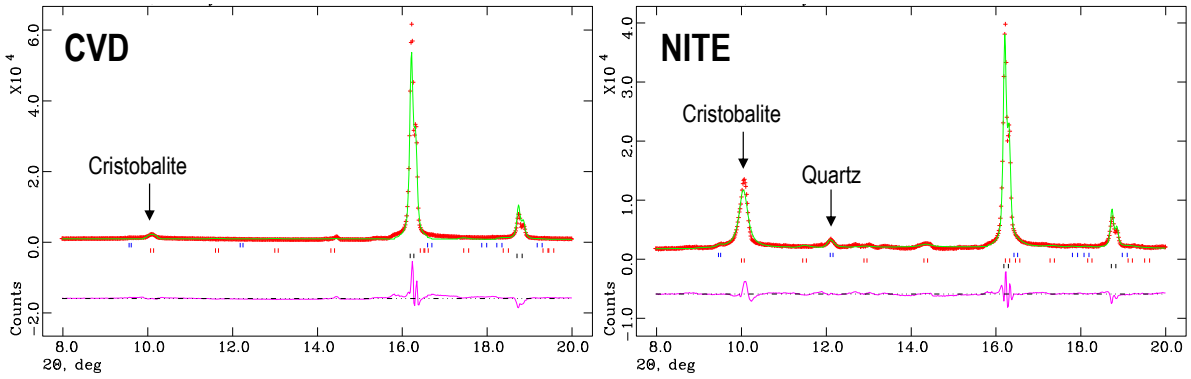

Fig. 10. X-ray diffraction of the surface oxide formed on CVD and NITE SiC specimens exposed to 1200°C steam at 3.4bar for 5 h. The larger peaks are due to the substrate.

Another class of SiC materials that may be of interest for this application is SiC/SiC composites with Nicalon fibers and a CVD SiC outer layer that protects the fibers from attack by oxidation. Figure 11 shows an example of a SiC/SiC composite specimen exposed for 24h at 1200°C in 3.4 bar steam. The recession on these specimens was similar to that observed for CVD SiC because the outer layer protected the fibers (and the BN fiber-matrix interlayer) from being rapidly attacked by the steam environment. Again, these observations are similar to prior work performed for gas turbine. applications[15,16].

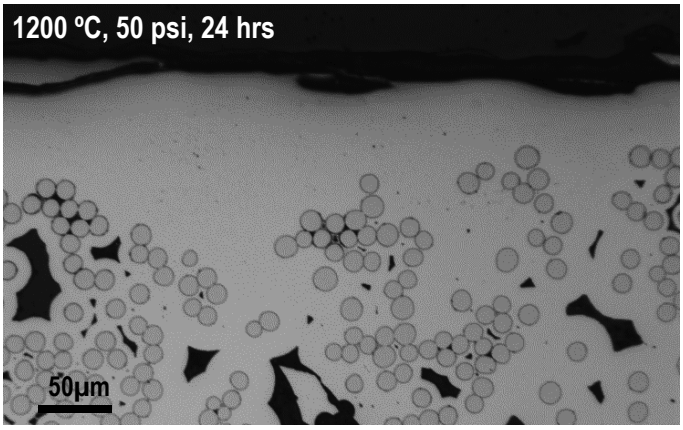

Fig. 11. SiC/SiC composite bar with protected SiC fibers exposed to 1200°C steam. The composite is not fully dense below the outer CVD SiC seal coat.

3.3 REACTION KINETICS

To determine the reaction rates at 1200°C, a time series of specimens was performed in 3.4 bar steam, Figure 12a. The data are plotted versus the square root of time to reflect the parabolic reaction rate expected for these materials. As mentioned previously, due to scale spallation, the mass change data may not be accurate and, clearly in some cases, spallation did occur, especially for the austenitic type 310 stainless steel which exhibited much lower mass gains than expected. The ferritic alloys AL294C and E-Brite both showed rate constants of 2-4 x 10^{-10} g^2/cm^4s consistent with chromia scale formation at 1200°C. For the slower growing alumina scale on APMT, the rate constant was 100 times lower than for chromia scales. To more accurately determine the reaction rates in the presence of steam, selected specimens were run in a TGA with 1 bar Ar-50%H_2O (it was not possible to achieve 100% steam in the TGA system), Figure 12b. As expected, the rates were similar in both conditions for APMT. However, the 310SS mass gain was much higher in the TGA experiment, comparable to the ferritic alloys in Figure 12a. Upon cooling, the 310SS specimen in the TGA spalled resulting in a mass loss. Likewise, the ferritic alloys showed slightly higher rates in the TGA experiment due to some degree of spallation in the high-pressure experiments. The mass gain for the SiC specimens was very different in the TGA experiment. The CVD specimen exhibited a low mass gain, likely due to the low gas flow rate and quartz reaction tube that precluded any accelerated material recession beyond formation of a silica scale by diffusional growth. In contrast, NITE SiC showed an initial high mass gain followed by a slower parabolic rate that was still higher than that observed for CVD SiC. This behavior is consistent with the thicker surface oxide observed on NITE SiC, Figure 9c.

The TGA allowed more accurate rate constants to be measured so a few samples were studied at 1000°-1200°C in order to quantify the effect of temperature. (The TGA quartz reaction tube limited the exposure temperature to 1200°C.) Figure 13a and Table 3 summarize some of the rate constants measured. The R^2 values in Table 3 provide an indication of the data fit when the mass gain data was plotted versus the square root of time[18]. The parabolic fits were better for the metals and less relevant for NITE and CVD SiC. As was shown in Figure 12b, the mass gain curves for NITE always showed initial high mass gains and were not parabolic in general. The CVD SiC data also could have been fit to a linear rate. Nevertheless, by using a parabolic rate throughout, the rates can be compared in Figure 13a. As expected, the rate on type 310 stainless steel was highest followed by the alumina-

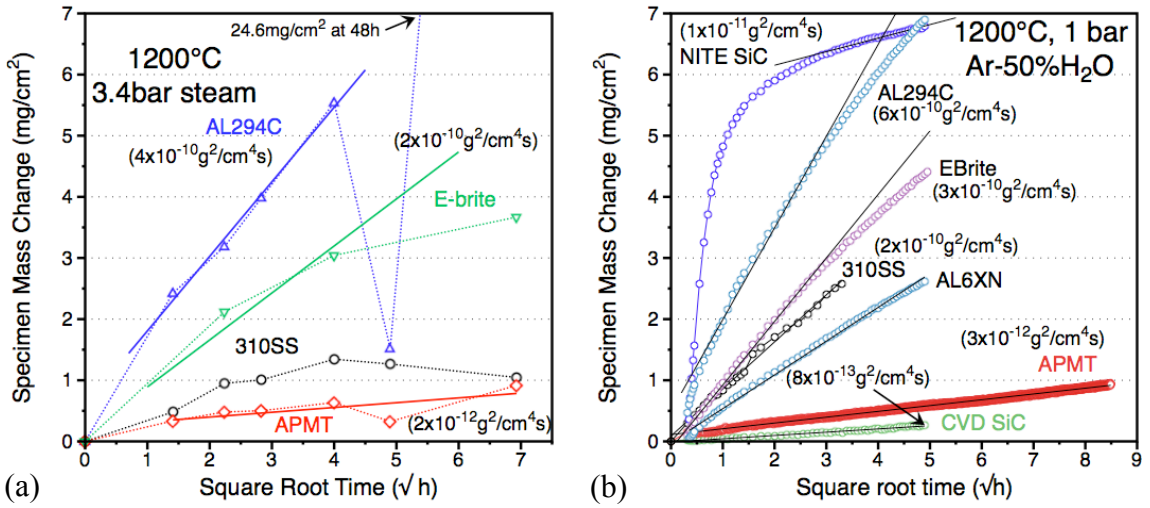

Fig. 12. Specimen mass change data for a series of specimens exposed at different times in (a) isothermal exposures in 3.4bar steam at 1200°C and (b) thermal gravimetric mass gain data at 1200°C in 1 bar Ar-50%H_2O.

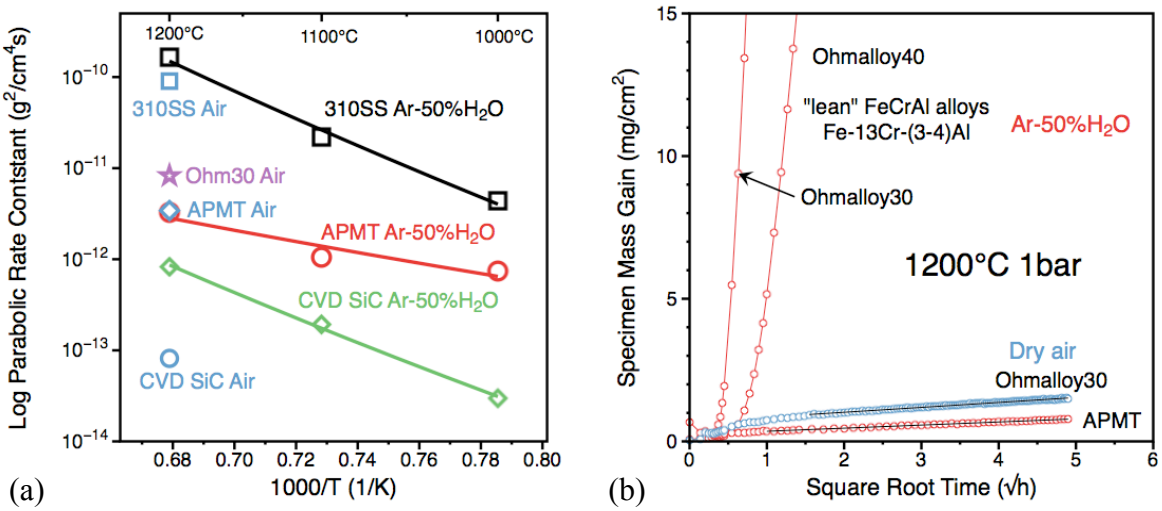

Fig. 13. (a) Arrhenius plot of the parabolic reaction rates for several materials and (b) comparison of mass gain for FeCrAl alloys at 1200°C in Ar-50%H_2O and dry air.

Table 3. Calculated parabolic rate constants from 24h TGA experiments in Ar-50%H_2O and dry air.

	1000°C H_2O	R^2	1000°C H_2O	R^2	1200°C H_2O	R^2	1200°C Air	R^2
CVD SiC	2.97E-14	0.345	1.92E-13	0.818	8.23E-13	0.986	8.16E-14	0.803
NITE	1.57E-09	0.993	3.64E-10	0.998	1.37E-11	0.984	1.47E-11	0.979
310SS	4.40E-12	0.997	2.19E-11	0.998	1.61E-10	0.995	9.03E-11	1.000
APMT	7.43E-13	0.964	1.05E-12	0.982	3.28E-12	0.997	3.42E-12	0.995
Ohmaloy30					breakaway		8.26E-12	0.994
Ohmaloy40					breakaway			
E-Brite					3.00E-10	0.997		
AL294C					6.25E-10	0.994		
AL6XN					8.46E-11	0.997		

forming FeCrAl alloy APMT. The slowest rates were measured for CVD SiC. To illustrate the effect of steam on the reaction rates, exposures also were made in dry air. While the reaction rates for APMT was very similar in air and steam (Table 3), the rates for 310SS and CVD SiC were both lower in dry air. The "lean" FeCrAl Ohmalloy alloys with only 13Cr (Table 1) showed breakaway oxidation at 1200°C in the TGA, indicating that a protective alumina scale could not be formed under these conditions, Figure 13b. However, in dry air a protective oxide was formed. The slightly higher rate constant for Ohmalloy 30 compared to APMT likely reflects the lack of a reactive element addition in the former. The Y and Hf in APMT is well known to reduce the rate constant at 1200°C by 2-3X[10,11].

For the TGA work, only chromia-forming 310SS was studied extensively while several more alloys were studied at 1200°C, Figure 12b and Table 3. In order to confirm that a similar ordering was observed in the higher pressure experiments, Figure 14 gives some examples of chromia scale thicknesses after 48h exposures at 1200°C in 3.4 bar steam. There was obvious scale spallation in some locations for the 310SS specimen, Figure 14a. The ferritic alloys formed more adherent oxides but significantly more internal oxidation was observed for the AL294C specimen (Fig. 14b), likely due to the presence of 0.4% Ti, 0.3%Si and 0.3%Nb in this alloy compared to E-Brite (0.2%Si and 0.1%Nb), which exhibited very little internal oxidation, Figure 14c. In this case, only a darker discontinuous phase at the chromia-metal interface was observed, likely SiO_2. Because silica is more thermodynamically stable than chromia, it can form beneath the chromia layer where the oxygen

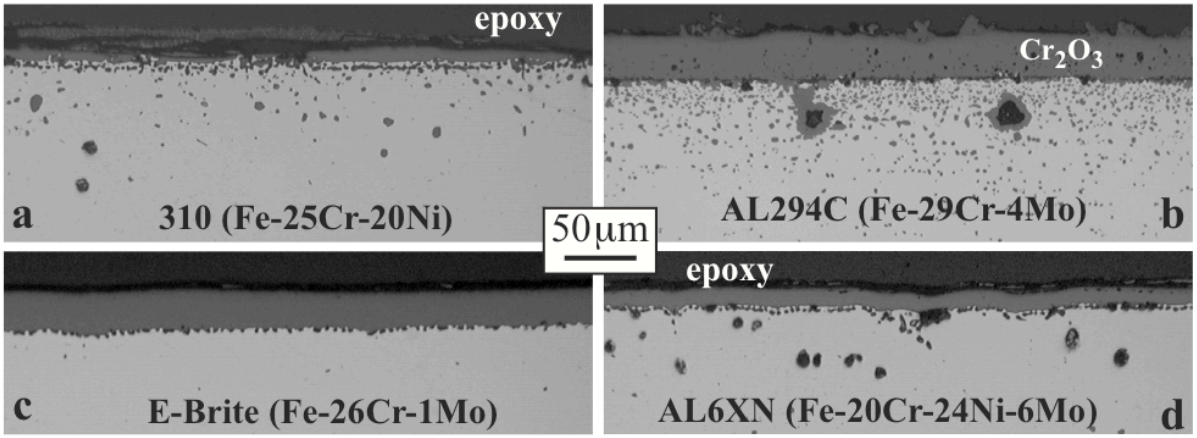

Fig. 14. Light microscopy of polished cross-sections after 48h at 1200°C in 3.4 bar steam (a) 310SS, (b) AL294C (c) E-Brite and (d) Fe-25Cr.

partial pressure is equal to the Cr/Cr_2O_3 equilibrium[19]. The scale thickness on E-Brite was very similar to the binary model Fe-25Cr alloy (not shown) that contained only 0.02%Si and did not show any indication of SiO_2 formation. This suggests that an inner silica layer is not truly protective in these conditions. Finally, Figure 14d shows the thinner scale formed on AL6XN, similar to the thinner scale formed on type 310 stainless steel. Both austenitic steels formed a thinner chromia layer but the scale appeared to be more adherent on AL6XN.

3.4 EFFECT OF ALLOY COMPOSITION ON OXIDATION RESISTANCE

A wider range of model alloys was exposed at a few conditions in order to understand which composition ranges are most resistant to these environments. Figure 15 summarizes a wide range of observations, mainly in 3.4 bar steam. The model Fe-Cr alloys were used to verify how much Cr would be needed for protective behavior. There has been considerable interest in using 9-14Cr ODS steels in nuclear applications, including fuel cladding[20-22]. However, prior work had shown that ODS Fe-13Cr had poor oxidation resistance in laboratory air above 900°C[23]. Figure 15b shows that Fe-15Cr was protective at 800°C but not at higher temperatures and Fe-20Cr showed higher mass gain at 1200°C indicating the onset of breakaway oxidation. The model and commercial alloys with higher Cr contents have shown protective behavior at 1200°C. Figure 16 shows examples of the breakaway oxidation for Fe-20Cr with large FeO_x nodules forming after only 2h at 1200°C in 3.4 bar steam, Figure 16a. However, in other areas, a protective chromia scale formed, Figure 16b. Larger nodules formed on Fe-15Cr under these conditions; however, a few areas could be found where a thin chromia scale formed, Figure 16c. There was not sufficient Cr in these alloys to retain protective scale formation. Even Fe-25Cr formed iron oxide in some locations after 48h at 1200°C and at higher temperatures, Figure 2.

Returning to Figure 15a, a series of model ternary Fe-20Cr-Ni alloys illustrated the benefit of higher Ni contents on oxidation resistance. While Ni is not desirable for fuel claddings because of its high neutron cross-section and formation of radioactive Co in the core, it does explain the relative performance of 304L/321L/347 with relatively low Ni contents and the superior performance of the high Ni austenitics such as HR120 and 310. Other elements besides Ni can improve the oxidation resistance of austenitic steels, especially Mn, Si and RE additions like La[24]. These elements result in

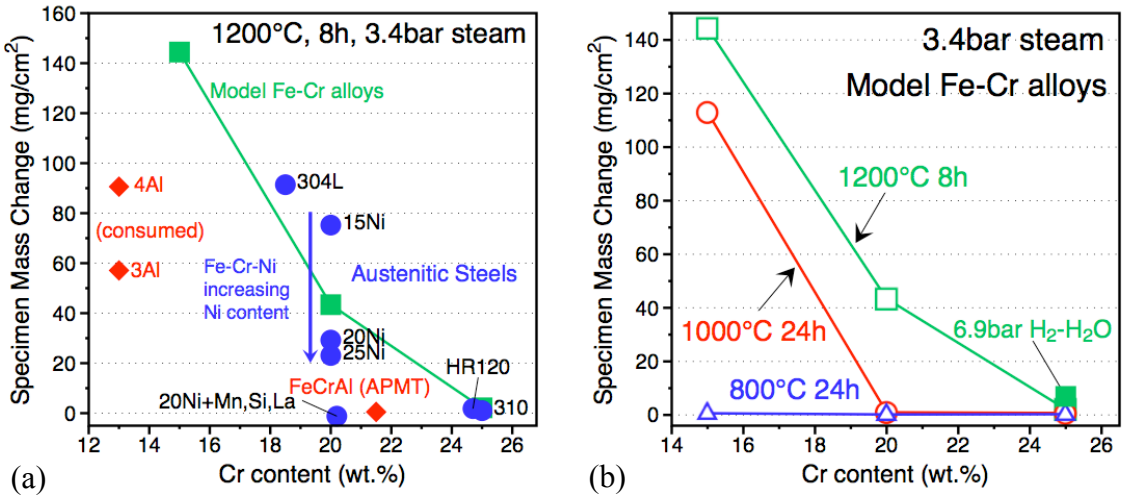

Fig. 15. Specimen mass change as a function of Cr content (a) after 8h at 1200°C in 3.4 bar steam and (b) Fe-Cr model alloys at 800°-1200°C.

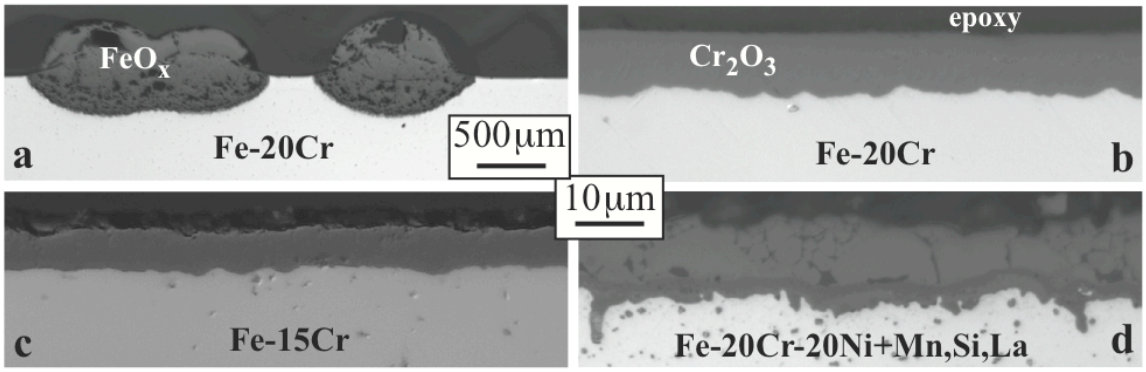

Fig. 16. Light microscopy of polished cross-sections of after exposure for 2h at 1200°C in 3.4bar steam (a) and (b) Fe-20Cr, (c) Fe-15Cr and (d) Fe-20Cr-20Ni+Mn,Si,La.

a more complex oxide (Figure 16d) but promote a more protective scale, particularly for the short time conditions of interest for this application.

Figure 15a also shows results for leaner FeCrAl compositions with 13Cr and 3-4%Al (Allegheny Ludlum Ohmalloy 30 and 40) alloys, as was shown at 1bar Ar-50%H_2O in Figure 13. These alloys are of interest because they are easier to fabricate and join than typical Fe-20Cr-5Al alloys and reflect the result of simply adding Al to current Fe-(9-14)Cr ODS alloys[25]. Somewhat surprisingly, these alloys were not able to form alumina at 1200°C in steam and were largely consumed during this exposure. This emphasizes the point that specific compositions with sufficient Cr and Al for protective behavior need to be defined for this application.

Figure 17 illustrates the benefit of Al in ODS alloys (only included in a few experiments because of limited availability). The Fe-14Cr ODM401 forms a protective oxide at 800° and 1000°C in 10.3bar of H_2-50%H_2O but not at 1200°C, Figure 17c. In contrast, ODS FeCrAl (PM2000) formed a thin protective oxide at all three conditions, Figures 17d-17f, very similar to APMT. In order to illustrate the protective behavior of PM2000, a ~100μm thick foil specimen also was exposed at 1200°C and formed a similar thin protective oxide as that on the 1.5mm thick specimen.

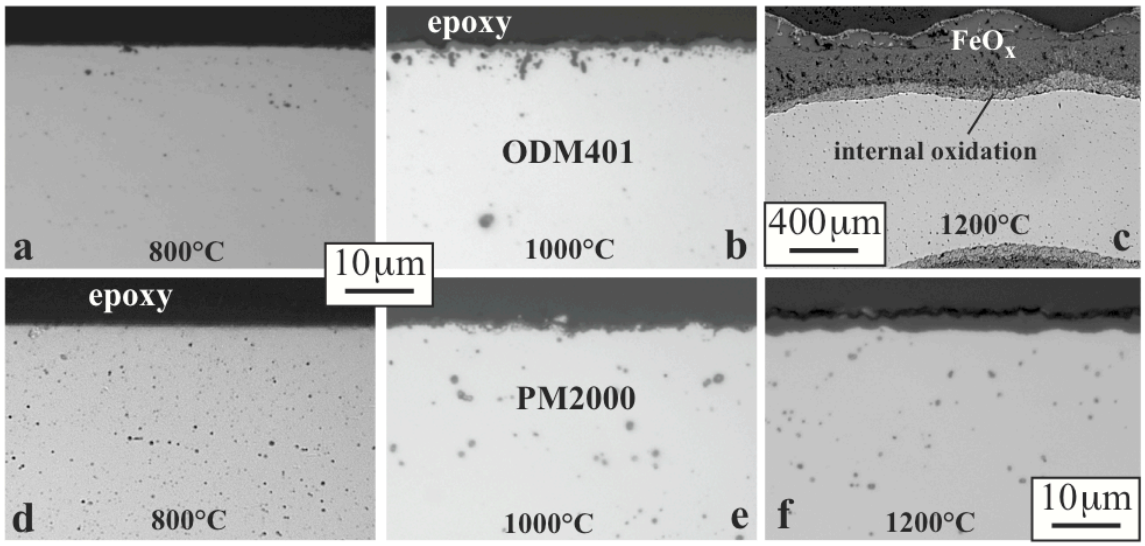

Fig. 17. Light microscopy of polished cross-sections after exposure for 8h in H_2-50%H_2O at 10.3bar at (a,d) 800°C, (b,e) 1000°C and (c,f) 1200°C for (a-c) ODM401 (ODS Fe-14Cr) and (d-f) PM2000 (ODS FeCrAl).

3.5 EFFECT OF PRESSURE AND HYDROGEN

Several additional experiments were conducted to evaluate the effect of pressure and H_2 in the environment, Table 2. For the most oxidation-resistant materials, there appeared to be little change with higher pressure and the addition of H_2. For example, the dashed line in Figure 2 shows the minor effect of higher total pressure with the addition of H_2. Likewise, Figure 15b shows only a slight change in the mass gain for Fe-25Cr for the 6.9 bar H_2-50%H_2O environment. A more substantial effect of pressure was observed for the lower alloyed steels. Figure 18 shows maximum metal loss results for the 317L tubing as a function of temperature and as a function of time at 1200°C. For this material that could not form a protective scale (based on the high mass gains), the

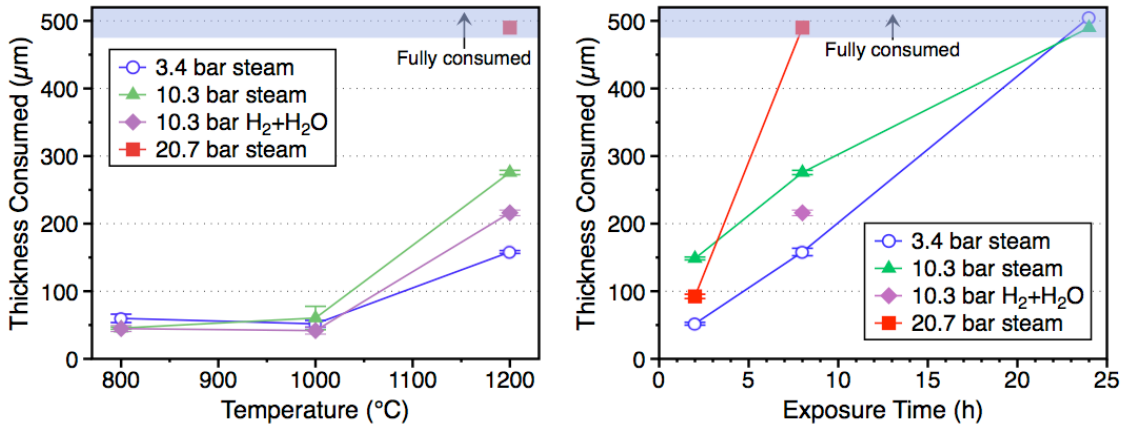

Fig. 18. Metal loss for 317L tubing in several pressures and two environments (a) as a function of temperature for 8h exposures and (b) as a function of time at 1200°C.

increased pressure appeared to accelerate the rate of metal loss at 1200°C. This effect is further illustrated in cross-sections in Figure 19 showing some of the images that were used to generate the metal loss data in Figure 18. (317L performed better than the other stainless steels tubes that were fully consumed after a similar exposure, Figure 3.) The laminated scales observed are typical of steels that rapidly oxidize in steam[26]. At 10.3 bar (150psi), switching from 100% H_2O to H_2-50%H_2O decreased the maximum metal loss, Figure 18. This difference can be seen in the cross-sections in Figures 19b and 19c and suggests that H_2-H_2O environments are not more aggressive than steam alone.

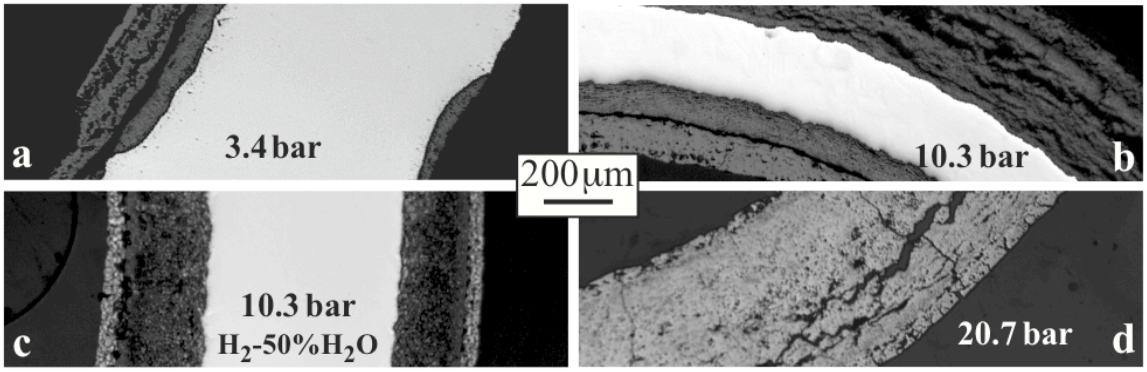

Fig. 19. Light microscopy of polished cross-sections of 317L tubing after 8h at 1200°C (a) 3.4 bar steam, (b) 6.9 bar steam, (c) 6.9 bar H_2-50%H_2O and (d) 20.7bar steam.

4. SUMMARY

Initial experiments were conducted at 800°-1350°C in 1-20 bar steam and H_2-H_2O environments to determine promising candidates for future study as more accident tolerant fuel claddings to replace zirconium alloys in light water reactors. Materials that can form protective alumina (such as FeCrAl) and silica (e.g. CVD SiC) showed minimal attack up to 1350°C in 3.4 bar steam. A range of commercial and model alloys were used to reach conclusions about the effects of alloy composition on steam oxidation resistance for this application. Conventional ~18Cr-10Ni stainless steels do not have sufficient oxidation resistance for the highest temperatures. However, higher alloyed steels such as 310 are much more oxidation resistant but not desirable due to their high Ni contents (and not as resistant as the alumina-forming alloys or SiC). At 1200°C, high (≥25% Cr) ferritic steels appear to be promising candidates for this application. Higher pressures and H_2 additions appeared to have minimal effect on the oxidation resistance of the most protective materials. However, these variables increased the maximum metal loss at 1200°C for 317L stainless steel. Several additional publications have already resulted from this study[27-29] and several more are in progress.

5. FUTURE WORK

Based on Table 2, the entire experimental space was not covered. However, a reasonable amount of data was collected to assess the effect of pressure and hydrogen on oxidation performance over this temperature range. Because of the concern about forming a Cr-rich α' phase under irradiation, lower Cr contents should be evaluated for both the Fe-Cr and Fe-Cr-Al compositions. The "lean" FeCrAl alloys did not perform well at 1200°C (Figures 13b and 15a), but intermediate compositions could be evaluated between 13-20%Cr and 3-5%Al. Lowering the Al content could improve the mechanical properties and weldability. For the Fe-Cr alloys, the binary model alloys provide important starting information. However, as was observed with the Fe-20Cr-20Ni alloy, additions of elements such as Mn, Si and La can substantially improve oxidation resistance (Figures 15a and 16d) in the presence of water vapor and reduce the critical amount of Cr needed for oxidation resistance[24]. Likewise, the ODS Fe-14Cr alloy performed better than the Fe-15Cr model alloy. For both Fe-Cr and Fe-Cr-Al alloys, ~400g castings can be made to evaluate composition effects in a limited number of future exposures.

Also, as this project concludes, somewhat limited characterization has been performed on the reaction products. Additional characterization of the surface oxide and internal oxidation will enhance the understanding of these results. However, the overall trends that FeCrAl alloys and high Cr ferritic alloys show the most promise for accident tolerant alloy claddings and SiC is promising as a ceramic cladding are not likely to change based on more characterization.

Substantial more work is needed to study the corrosion resistance and mechanical behavior in pressurized boiling water at up to 320°C and the effects of irradiation on these alloys (especially α' formation under irradiation) because these alloys have not been previously considered for fuel cladding applications.

6. REFERENCES

1. P. Yvon and F. Carré, *Journal of Nuclear Materials,* **385**, 217 (2009).
2. L. Hallstadius, S. Johnson, E. Lahoda, *Progress in Nuclear Energy*, **57**, 71 (2012).
3. Y. Katoh, L.L. Snead, I. Szlufarska, W.J. Weber, *Current Opinion in Solid State and Materials Science*, 16, 143 (2012)
4. E. J. Opila, *Materials Science Forum*, **461-464**, 765 (2004).
5. J.E. Rivera and J.E. Meyer, MIT-EL Report #80-021, Cambridge, MA, July 1980.
6. V. F. Urbanic and T. R. Heidrick, *Journal of Nuclear Materials*, **75**, 251 (1978).
7. R. E. Pawel, J. V. Cathcart and R. A. McKee, *Journal of The Electrochemical Society*, **126**, 1105 (1979).
8. M. Moalem, D.R. Olander, *Journal of Nuclear Materials*, **182**, 170 (1991).
9. R. Peraldi and B. A. Pint, *Oxidation of Metals*, **61**, 463 (2004).
10. B. A. Pint, *Oxidation of Metals*, **45**, 1 (1996).
11. B. A. Pint, *Journal of the American Ceramic Society*, **86**, 686 (2003).
12. E. J. Opila and R. E. Hann Jr., *Journal of the American Ceramic Society*, **80**, 197 (1997).
13. E. J. Opila, *Journal of the American Ceramic Society*, **82**, 625 (1999).
14. R. Robinson and J. L. Smialek, *Journal of the American Ceramic Society*, **82,** 1817 (1999).
15. P. F. Tortorelli and K. L. More, *Journal of the American Ceramic Society*, **86**, 1249 (2003).
16. K. L. More, P. F. Tortorelli, L. R. Walker, N. Miriyala, J. R. Price and M. van Roode, *Journal of the American Ceramic Society*, **86,** 1272 (2003).
17. C. S. Tedmon, *Journal of the Electrochemical Society* **113**, 766 (1966).
18. B. Pieraggi, *Oxidation of Metals*, **27**, 177 (1987).
19. R. C. Lobb, J. A. Sasse and H. E. Evans, *Materials Science and Technology*, **5**, 828 (1989).
20. S. Ukai, M. Harada, H. Okada, M. Inoue, S. Nomura, S. Shikakura, K. Asabe, T. Nishida and M. Fujiwara, *Journal of Nuclear Materials*, **204**, 65 (1993) 65-73.
21. G. R. Romanowski, L. L. Snead, R. L. Klueh and D. T. Hoelzer, *Journal of Nuclear Materials*, **283-287**, 642 (2000).
22. R. L. Klueh, J. P Shingledecker, R. W. Swindeman, D. T. Hoelzer, *Journal of Nuclear Materials*, **341**, 103 (2005).
23. B. A. Pint and I. G. Wright, *Oxidation of Metals*, **63**, 193 (2005).
24. B. A. Pint, R. Peraldi and P. J. Maziasz, *Materials Science Forum*, **461-464**, 815 (2004).
25. J. H. Lee, R. Kasada, A. Kimura, T. Okuda, M. Inoue, S. Ukai, S. Ohnuki, T. Fujisawa and F. Abe, *Journal of Nuclear Materials*, **417**, 1225 (2011).
26. I. G. Wright and R. B. Dooley, *International Materials Reviews*, **55** (3), 129 (2010).
27. T. Cheng, J. R. Keiser, M. P. Brady, K. A. Terrani and B. A. Pint, *Journal of Nuclear Materials*, **427** (2012) 396-400.
28. B. A. Pint, M. P. Brady, J. R. Keiser, T. Cheng and K. A. Terrani (2012) "High Temperature Oxidation of Fuel Cladding Candidate Materials in Steam-Hydrogen Environments," in *Proceedings of the 8th International Symposium on High Temperature Corrosion and Protection of Materials*, Les Embiez, France, May 2012, Paper#89.
29. K. A. Terrani, G. W. Chinthaka Silva, J. R. Keiser, M. P. Brady, T. Cheng, B. A. Pint and L. L. Snead, "High Temperature Oxidation of SiC and Advanced Fe-Based Alloys in Steam-Hydrogen Environments," submitted to the proceedings of Top Fuel 2012.